Coherence Imaging System

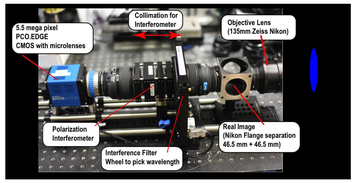

Measures the spectral coherence of an emission line using an imaging interferometer of fixed delay (See D. Ennis - CP11.00061)

Measurements of ion parameters in both the edge and the core of CTH plasmas beneficial for island divertor and MHD mode-locking experiments

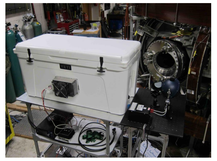

Instrument is housed in a marine cooler to reduce temperature fluctuations of the interferometer crystal

Peltier cooler with feedback controls the ambient temperature (~23 °C) inside the marine cooler

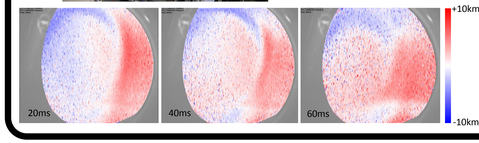

Changes in toroidal flow over time

Spectroscopic Studies Support DIII-D and Others

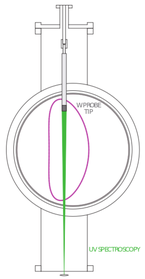

High-Z materials exposed to plasma on CTH to improve spectroscopic erosion measurements through the S/XB method (See C. Johnson - NP11.00080)

New Mo, W atomic calculations completed at Auburn allowing more accurate erosion measurements (See S. Loch - NP11.000801)

W, Mo, SiC, and stainless steel probes inserted into CTH with collection optics opposing probe

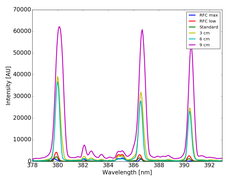

Probe depth scan allows for lines to be distinguished from base CTH impurities

Collisional radiative code developed to model spectra and compare with experiment

Using SXR measurements in V3FIT reconstructions yields more accurate current profiles

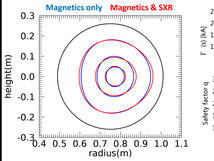

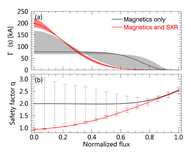

Plasma current is more concentrated in the center (top) dropping the central q value (bottom) when SXR signals are included in the V3FIT reconstruction (See X.Ma CP11.00062)

Flux surfaces at φ=π/10 show more elongation when SXR signals are included in the reconstruction

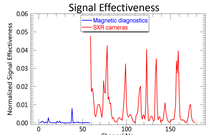

Internal SXR measurements have more influence on central current distribution than external magnetic signals

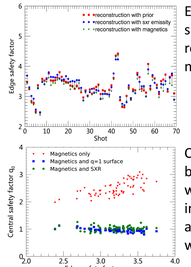

Edge Safety factor is similar for all three reconstruction methods.

Central Safety factor is better determined with the use of SXR inversion information and SXR signals than with magnetics alone.

Reduction of vertical drift rate with addition of 3D fields

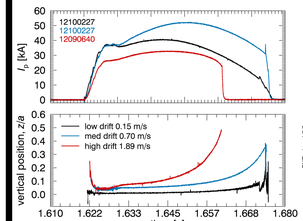

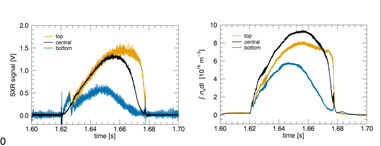

Vertical motion detected by magnetic, SXR, and interferometric diagnostics

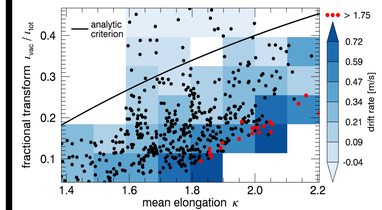

Discharges exhibit faster drift Rates at higher elongation and At lower fractional transform

Plasmas with high elongation are stabilized with the addition of vacuum transform

Qualitative agreement with Analytic criterion for vertical stability

Control of Sawtooth dynamics with 3D fields

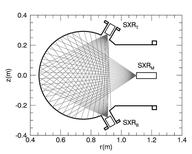

Central SXR camera used in this study

Biorthogonal/SVD analysis used to help identify the inversion radius

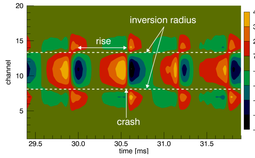

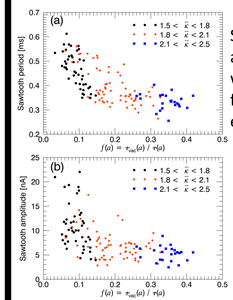

Sawtooth period (a) and amplitude (b) decrease with increasing fractional transform and elongation

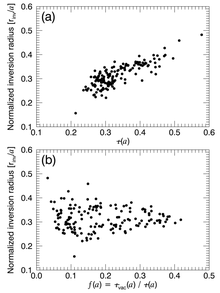

Sawtooth inversion radius increases with (a) increasing total transform, but not with (b) fractional transform

CTH has a flexible coil set that allows for exploration of multiple magnetic field configurations

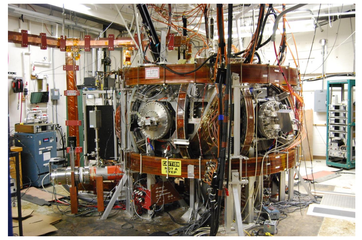

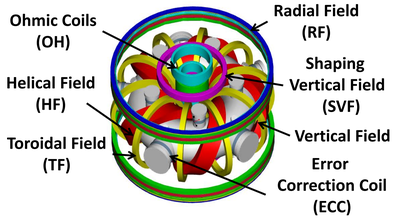

Typical CTH parameters

5 field periods		discharge duration ~0.1s	
R_o	= 0.75 m	n_e	≤ 5 x 10^{19} m^{-3}
a_{vessel}	= 0.29 m	T_e	≤ 200 eV
a_{plasma}	≤ 0.2m		
B_o	≤ 0.7 T		
P_{input}	≤ 15 kW ECRH ~ 200kW OH	I_p	≤ 80 kA
	~ 150 kW 2nd Harmonic x-mode (under construction)		
Vacuum transform 0.02 – 0.35		<β>	≤ 0.2%

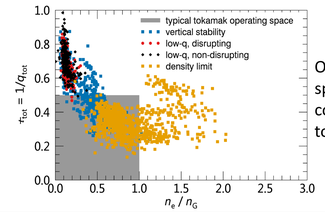

Operational space of CTH compared to tokamak

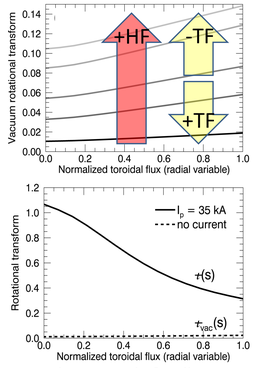

CTH has control of stellarator transform. Transform with plasma current is tokamak-like

Addition of stellarator transform increases operational density

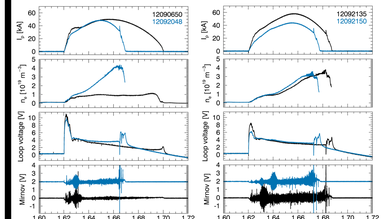

With similar plasma current history, increased fueling results in disruption

Shots with lower plasma current disrupt at similar densities

Current profile at disruption narrows to a greater extent as the external transform is raised

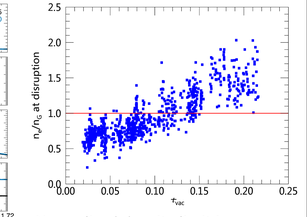

Normalized density limit increases by a factor of nearly 4 as the vacuum transform is raised

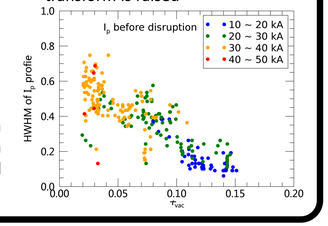

Thomson diagnostic has detected Raman Scattering

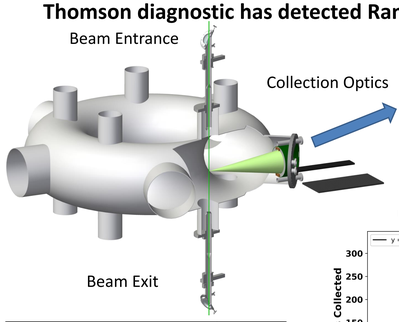

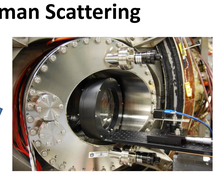

Laser energy	1.7 J
Scattering wavelength	532 nm
PMT active area	19.63 mm^2
Estimated excess noise factor	~ 1.6
Average PMT quantum efficiency	~ 0.39
Estimated system transmission	~ 0.37
$\frac{\text{Total photo-electrons}}{10^{19}\ \text{plasma e-}}$	~ 10^4
$\frac{\text{Total electrons collected per channel}}{10^{19}\ \text{plasma e-}}$	~ 10^3
S/N ratio per channel	~ 8 to 40

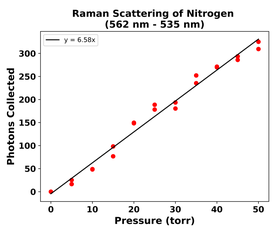

Raman scattering is linear with background N2 pressure (See P.J. Traverso - CP11.00060)

VGA-8050M pulsed gyrotron oscillator 200kW - 28GHz 75ms

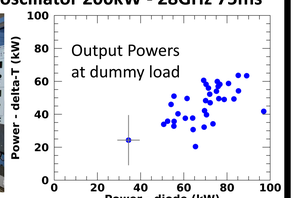

Interferometer being upgraded to five channels

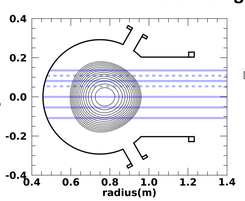

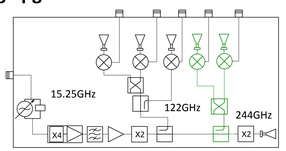

Additional channels will give better resolution of the density profile

Mode structure modeled with current filaments

MHD perturbed currents can be approximated as being parallel to magnetic field lines on mode resonant rational surface

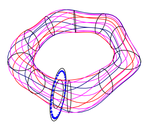

Current filaments follow B-field lines

$$S_i^M = \sum_{j=0}^{N_f} M_{ij} I_j$$

$$I_j = I_0 \sin(m\theta_j + \delta)$$

Results from χ^2 fit of I_0 and δ

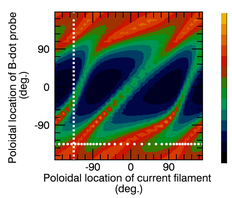

Mutual inductance measures the response of the B-dot probes to the currents

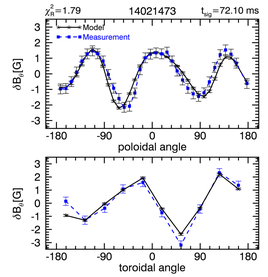

Low-q disruptions cease when $t_{vac}(a) > 0.07$

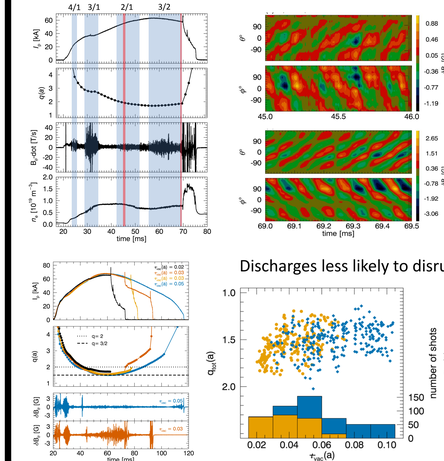

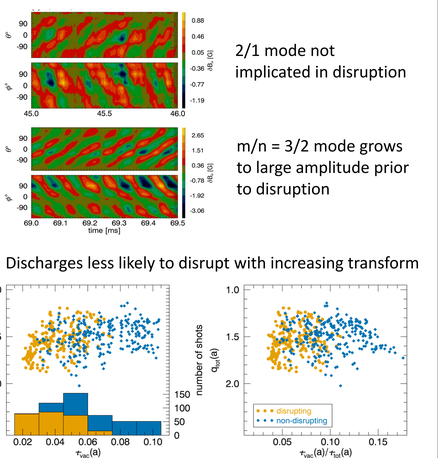

2/1 mode not implicated in disruption

m/n = 3/2 mode grows to large amplitude prior to disruption

Discharges less likely to disrupt with increasing transform